

What happens to the Υ and η_b in the quark-gluon plasma? Bottomonium spectral functions from lattice QCD

G. Aarts^a, C. Allton^a, S. Kim^{b,a}, M. P. Lombardo^{c,d}, M. B. Oktay^e,
S. M. Ryan^f, D. K. Sinclair^g and J.-I. Skullerud^h

^a*Department of Physics, Swansea University, Swansea, United Kingdom*

^b*Department of Physics, Sejong University, Seoul 143-747, Korea*

^c*INFN-Laboratori Nazionali di Frascati, I-00044, Frascati (RM) Italy*

^d*Humboldt-Universität zu Berlin, 12489 Berlin, Germany*

^e*Physics Department, University of Utah, Salt Lake City, Utah, USA*

^f*School of Mathematics, Trinity College, Dublin 2, Ireland*

^g*HEP Division, Argonne National Laboratory, 9700 South Cass Avenue
Argonne, Illinois 60439, USA*

^h*Department of Mathematical Physics, National University of Ireland Maynooth
Maynooth, County Kildare, Ireland*

September 21, 2011

Abstract

We study bottomonium spectral functions in the quark-gluon plasma in the Υ and η_b channels, using lattice QCD simulations with two flavours of light quark on highly anisotropic lattices. The bottom quark is treated with nonrelativistic QCD (NRQCD). In the temperature range we consider, $0.42 \leq T/T_c \leq 2.09$, we find that the ground states survive, whereas the excited states are suppressed as the temperature is increased. The position and width of the ground states are compared to analytical effective field theory (EFT) predictions. Systematic uncertainties of the maximum entropy method (MEM), used to construct the spectral functions, are discussed in some detail.

1 Introduction

Quarkonia (heavy quark–antiquark bound states) are among the most important probes of the hot medium created in relativistic heavy ion collisions. Unlike light quarks, heavy quarks are predominantly created in the primordial hard collisions, and do not reach chemical equilibrium with the medium. Since J/ψ suppression was proposed in 1986 as a signature of the formation of the quark-gluon plasma [1], the charmonium system has been investigated intensively, both experimentally [2,3] and theoretically [4,5]. With the advent of the Large Hadron Collider, there has been increasing interest in bottomonium states as well, since b quarks are now for the first time being produced copiously in heavy ion collisions. In particular, the recent results from CMS indicate the survival of the $\Upsilon(1S)$ state, but suppression of the $\Upsilon(2S + 3S)$ states [6] (see Ref. [7] for results from STAR). A number of phenomenological studies have since attempted to explain this suppression pattern [8,9]. It is generally expected that bottomonium provides a cleaner probe than charmonium, since statistical recombination of independent quarks and antiquarks plays a much less important role, and also since b quarks retain their nature as ‘hard probes’ to a larger extent. Cold nuclear matter effects are also expected to be simpler for b than for c quarks.

Theoretically, quarkonium suppression has traditionally been investigated with potential models (see e.g. Refs. [10,11] and references therein) and with lattice QCD computations of quarkonium spectral functions [12–19]. Exploiting the strongly-coupled nature of the quark-gluon plasma, studies using gauge-gravity duality have also been used, see e.g. Refs. [20–22] for recent results. Other studies can be found in Refs. [23,24]

In the past few years, the theoretical understanding of quarkonium melting and in-medium modification has been improved substantially by casting the problem in the language of effective field theories (EFTs) [25–35]. By relying on scale separation between the heavy quark mass M and the temperature T of the quark-gluon plasma and on weak coupling to distinguish the inverse system size $M\alpha_s$, the binding energy $M\alpha_s^2$ and the inverse Debye screening length $m_D \sim \sqrt{\alpha_s}T$, a series of EFTs can be written down. One of the main outcomes of this formulation is the appearance of a complex heavy quark potential, where the imaginary part is generated by integrating out thermal fluctuations. For complex potential model studies, see e.g. Refs. [36,37] as well as those listed above. Attempts at extracting the complex potential from lattice QCD can be found in Refs. [38,39].

Various sequences of EFTs can be constructed, depending on the ordering of the scales. For instance, Refs. [25–27] have focused on high temperature, where the bound state is about to fall apart, employing

$$M \gg T > M\alpha_s > m_D \gg M\alpha_s^2. \quad (1.1)$$

The corresponding bound state spectral functions are then considerably affected by the presence of the quark-gluon plasma. On the other hand, in Ref. [31] lower

temperatures are considered, using

$$M \gg M\alpha_s \gg T \gg M\alpha_s^2 \gg m_D. \quad (1.2)$$

In this case the ground states are less affected and thermal effects can be cast in terms of thermal mass shifts and widths.

In all cases, integrating out the heavy quark mass scale M yields nonrelativistic QCD (NRQCD) as an effective field theory. The appearance of further EFTs depends on the ordering of the scales and weak coupling. Since the applicability of weak coupling arguments is not guaranteed for temperatures up to $2 - 3T_c$, where T_c is the transition temperature between the hadronic phase and the quark-gluon plasma, it would be desirable to solve NRQCD in the quark-gluon plasma nonperturbatively, using lattice QCD simulations at finite temperature. This programme was recently initiated by us.¹

In Ref. [41] we studied S and P wave bottomonium correlators at four different temperatures, $T/T_c = 0.42, 1.05, 1.40$ and 2.09 , using NRQCD for the heavy quark dynamics and relativistic two-flavour lattice simulations for the quark-gluon system. The main result of that analysis was the presence of strong temperature dependence in the P wave correlators (in the $\chi_{b1,b2,b3}$ channels), indicating a melting of P wave bound states in the quark-gluon plasma. At the highest temperature, we found the behaviour of the P wave correlators to be consistent with nearly-free dynamics of the heavy quarks.

The temperature dependence in the S wave correlators was much less visible. The goal of this paper is to analyse in detail the S wave correlators, in the vector (Υ) and pseudoscalar (η_b) channels, and construct the corresponding spectral functions at several temperatures in the hadronic phase and the quark-gluon plasma. Our main results can be seen in Fig. 4, which shows that as the temperature is increased the ground state peaks of the Υ and η_b remain visible, even though they broaden and reduce in height, while their excited states become suppressed at higher temperature and are no longer discernible at $T/T_c \sim 1.68$. The temperature dependence of the position and width of the ground state peaks is compared to analytical predictions obtained within the EFT formalism [31]. We note that the survival of the $\Upsilon(1S)$ state and suppression of excited states is consistent with the recent CMS and STAR results [6, 7].

This paper is organised as follows. In the following section we describe NRQCD as an effective field theory for QCD, focusing on finite temperature aspects. We discuss in particular how the nonrelativistic formulation has several advantages compared to standard relativistic dynamics at nonzero temperature. Lattice details are collected in Sec. 3. The main part of the paper starts in Sec. 4, where the high-precision euclidean correlators in the Υ and η_b channels are presented. The corresponding spectral functions are shown in Sec. 5. Here we also compare

¹See Ref. [40] for an early pioneering study.

our results with analytical EFT predictions. A discussion of the maximum entropy method [42], used to construct the spectral functions, and of systematic uncertainties is given in Sec. 6. We summarise in Sec. 7. The Appendix contains an analysis of lattice artefacts in NRQCD spectral functions in the absence of interactions. Some preliminary results have previously been presented in Ref. [43].

2 NRQCD at nonzero temperature

NRQCD is an effective theory of QCD where physics above the scale of the heavy quark mass is integrated out [44–47]. It differs from heavy quark effective theory (HQET) in that terms in the NRQCD lagrangian are ordered in powers of $v = |\mathbf{p}|/M$, the typical velocity of a heavy quark in the heavy quarkonium rest frame. In principle, there are infinitely many terms in such an expansion and taking into consideration more terms would mean more accurate relativistic corrections. However, in practice, only a small number of terms is necessary for a given accuracy, since v^2 is small (~ 0.1 for the bottom quark) and the series converges quickly. Also, including more terms in an effective theory would normally mean tuning more coefficients, resulting in a loss of predictive power. In practice, the coefficients of the NRQCD lagrangian can be calculated using perturbation theory since M is large (~ 5 GeV for the bottom quark) and often tree level values are sufficient when simulation parameters are chosen judiciously.

In this work, we use the following $\mathcal{O}(v^4)$ euclidean NRQCD lagrangian density for the bottom quark [46],

$$\mathcal{L} = \mathcal{L}_0 + \delta\mathcal{L}, \quad (2.1)$$

with

$$\mathcal{L}_0 = \psi^\dagger \left(D_\tau - \frac{\mathbf{D}^2}{2M} \right) \psi + \chi^\dagger \left(D_\tau + \frac{\mathbf{D}^2}{2M} \right) \chi, \quad (2.2)$$

and

$$\begin{aligned} \delta\mathcal{L} = & -\frac{c_1}{8M^3} [\psi^\dagger (\mathbf{D}^2)^2 \psi - \chi^\dagger (\mathbf{D}^2)^2 \chi] \\ & + c_2 \frac{ig}{8M^2} [\psi^\dagger (\mathbf{D} \cdot \mathbf{E} - \mathbf{E} \cdot \mathbf{D}) \psi + \chi^\dagger (\mathbf{D} \cdot \mathbf{E} - \mathbf{E} \cdot \mathbf{D}) \chi] \\ & - c_3 \frac{g}{8M^2} [\psi^\dagger \boldsymbol{\sigma} \cdot (\mathbf{D} \times \mathbf{E} - \mathbf{E} \times \mathbf{D}) \psi + \chi^\dagger \boldsymbol{\sigma} \cdot (\mathbf{D} \times \mathbf{E} - \mathbf{E} \times \mathbf{D}) \chi] \\ & - c_4 \frac{g}{2M} [\psi^\dagger \boldsymbol{\sigma} \cdot \mathbf{B} \psi - \chi^\dagger \boldsymbol{\sigma} \cdot \mathbf{B} \chi]. \end{aligned} \quad (2.3)$$

Here D_τ and \mathbf{D} are gauge covariant temporal and spatial derivatives, ψ is the heavy quark and χ is the heavy anti-quark. The coefficients $c_i = 1$ at tree level.

In contrast to the relativistic theory, the time evolution for nonrelativistic heavy quarks is an initial value problem. In particular, the presence of a nonzero temperature is not imposed as a boundary condition in the temporal direction

of the heavy quark field. Instead, the effects of temperature enter for the heavy quarks as they propagate through the thermal medium of light quarks and gluons. Since we are considering temperatures $T \ll M$, we expect that finite temperature can be taken into account without affecting the effective field theory nature of NRQCD.

The absence of thermal boundary conditions simplifies spectral relations considerably. In the relativistic formulation, the euclidean correlator and its spectral function are related via

$$G(\tau) = \int_{-\infty}^{\infty} \frac{d\omega}{2\pi} K(\tau, \omega) \rho(\omega), \quad (2.4)$$

with the kernel

$$K(\tau, \omega) = \frac{\cosh[\omega(\tau - 1/2T)]}{\sinh(\omega/2T)}. \quad (2.5)$$

Temperature dependence enters in two ways: kinematically due to the periodic boundary conditions, reflected in the periodicity of the kernel, and dynamically due to the propagation through a temperature-dependent medium. It is important to disentangle these two, since the first one is present even in the absence of interactions and does not reflect the effects of the thermal medium.

In NRQCD the kinematical temperature dependence is absent. This can be seen in a number of ways. Following Ref. [27], we write $\omega = 2M + \omega'$ and drop terms that are exponentially suppressed when $M \gg T$. The spectral relation (2.4) then reduces to

$$G(\tau) = \int_{-2M}^{\infty} \frac{d\omega'}{2\pi} \exp(-\omega'\tau) \rho(\omega') \quad (\text{NRQCD}), \quad (2.6)$$

even at nonzero temperature. This reflects the fact that the NRQCD propagator is constructed from an initial-value problem. Physically it implies that the heavy quarks are not in thermal equilibrium with the light-quark–gluon system, but instead appear as probes.

This simplification also removes the problems associated with the so-called constant contribution [48]. In the small energy limit, the product of the relativistic kernel and the spectral density is independent of euclidean time [49],

$$\lim_{\omega \rightarrow 0} K(\tau, \omega) \rho(\omega) = 2T \frac{\rho(\omega)}{\omega} \Big|_{\omega=0}, \quad (2.7)$$

where we used that the spectral function $\rho(\omega)$ is an odd function in ω and increases linearly at small ω . This is relevant for transport coefficients [49] and for conserved charges, in the presence of which spectral functions will have a contribution of the form

$$\rho(\omega) = \chi 2\pi\omega\delta(\omega) + \text{contribution at larger } \omega, \quad (2.8)$$

where χ is a susceptibility. Spectral weight at vanishing energy will therefore yield a constant, additive contribution to the euclidean correlator. It has been argued [48, 50] that this constant contribution interferes with the interpretation of charmonium survival or melting, as seen by lattice QCD simulations [12–19]. It also requires a modification [51] of Bryan’s algorithm in the implementation of the maximum entropy method [42, 52]. In NRQCD, the contribution at small energies is absent, since only energies above $2M$ are present.² In summary, in the heavy quark limit the spectral relation simplifies considerably, removing the problems associated with thermal boundary conditions. All temperature effects seen in the correlators are thus due to changes in the light-quark–gluon system.

3 Lattice formulation

We solve NRQCD nonpertubatively using lattice QCD, and let the bottom quarks propagate through a medium of gluons and two flavours of light quark. Gauge configurations with $N_f = 2$ dynamical light Wilson-type quark flavours are produced on highly anisotropic lattices ($\xi \equiv a_s/a_\tau = 6$) of size $N_s^3 \times N_\tau$. A summary of the lattice datasets is given in Table 1, while more details of the lattice action and parameters can be found in Refs. [16, 55]. In the light quark sector, $m_\pi/m_\rho \simeq 0.54$, which implies that the light quark masses are comparable to the strange quark mass.

N_s	N_τ	$T(\text{MeV})$	T/T_c	N_{cfg}
12	80	90	0.42	250
12	32	230	1.05	1000
12	28	263	1.20	1000
12	24	306	1.40	500
12	20	368	1.68	1000
12	18	408	1.86	1000
12	16	458	2.09	1000

Table 1: Summary of the lattice data set. The lattice spacing is set using the $1P-1S$ spin-averaged splitting in charmonium [17], corresponding to $a_s \simeq 0.162\text{fm}$, $a_\tau^{-1} \simeq 7.35 \text{ GeV}$. The anisotropy is $a_s/a_\tau = 6$.

In Ref. [41] we studied the effect of temperature on S and P wave bottomonium correlators. Compared to that study, we have greatly increased the number of configurations and expanded the number of temperature values (in Ref. [41] we only considered $T/T_c = 0.42, 1.05, 1.40$ and 2.09). We have also improved the nonperturbative tuning of the bare anisotropy in the action.³

²Heavy quark diffusion has been studied using heavy quark effective theory [53, 54].

³All data analysed here correspond to Run 7 in the terminology of Ref. [16].

In order for NRQCD to be a consistent effective field theory in a lattice simulation, the lattice spacing a_s , acting as a short-distance cutoff, has to be kept finite and satisfy $Ma_s \sim 1$. Finite lattice spacing errors can then be systematically improved as they appear at the same order as relativistic effects due to $a_s \sim 1/M$. There are many equivalent discretizations of the continuum NRQCD lagrangian density discussed above. Following earlier studies of heavy quarkonium spectroscopy at zero temperature [56–58], we calculate the heavy quark Green function on an anisotropic lattice using

$$\begin{aligned} G(\mathbf{x}, \tau = 0) &= S(\mathbf{x}), \\ G(\mathbf{x}, \tau = a_\tau) &= \left(1 - \frac{H_0}{2n}\right)^n U_4^\dagger(\mathbf{x}, 0) \left(1 - \frac{H_0}{2n}\right)^n G(\mathbf{x}, 0), \\ G(\mathbf{x}, \tau + a_\tau) &= \left(1 - \frac{H_0}{2n}\right)^n U_4^\dagger(\mathbf{x}, \tau) \left(1 - \frac{H_0}{2n}\right)^n (1 - \delta H) G(\mathbf{x}, \tau), \end{aligned} \quad (3.1)$$

where $S(\mathbf{x})$ is the source, the lowest-order hamiltonian reads

$$H_0 = -\frac{\Delta^{(2)}}{2M}, \quad (3.2)$$

and

$$\begin{aligned} \delta H &= -\frac{(\Delta^{(2)})^2}{8M^3} + \frac{ig}{8M^2}(\boldsymbol{\Delta} \cdot \mathbf{E} - \mathbf{E} \cdot \boldsymbol{\Delta}) - \frac{g}{8M^2} \boldsymbol{\sigma} \cdot (\boldsymbol{\Delta} \times \mathbf{E} - \mathbf{E} \times \boldsymbol{\Delta}) \\ &\quad - \frac{g}{2M} \boldsymbol{\sigma} \cdot \mathbf{B} + \frac{a_s^2 \Delta^{(4)}}{24M} - \frac{a_s (\Delta^{(2)})^2}{16nM^2}. \end{aligned} \quad (3.3)$$

The integer n controls the high-momentum behaviour of the evolution equation. Since the bottom quark is heavy enough, we take $n = 1$. The last two terms in δH are corrections to the kinetic energy term at finite lattice spacing [45]. The lattice covariant derivatives are defined as

$$\begin{aligned} \Delta_i \psi &= \frac{1}{2a_s} \left[U_i(x) \psi(x + \hat{i}) - U_i^\dagger(x - \hat{i}) \psi(x - \hat{i}) \right], \\ \Delta^{(2)} \psi &= \sum_i \Delta_i^{(2)} \psi = \sum_i \frac{1}{a_s^2} \left[U_i(x) \psi(x + \hat{i}) - 2\psi(x) + U_i^\dagger(x - \hat{i}) \psi(x - \hat{i}) \right], \\ \Delta^{(4)} \psi &= \sum_i (\Delta_i^{(2)})^2 \psi, \end{aligned} \quad (3.4)$$

and \mathbf{E} and \mathbf{B} in Eq. (3.3) are lattice definitions of the chromoelectric and chromomagnetic fields. We use tadpole improvement [59]:

$$U_i(x) \rightarrow \frac{U_i(x)}{u_s}, \quad U_0(x) \rightarrow \frac{U_0(x)}{u_\tau}, \quad (3.5)$$

where $u_{s,\tau}$ are the average space-like (s) and time-like (τ) links, determined from the plaquette expectation values; although in practice, the time-like mean link u_τ is set to 1. The coefficients c_i are then set to 1. Note that $u_s \neq u_\tau$, since the lattice is anisotropic.

An accurate determination of bottomonium spectroscopy requires careful tuning of the bare heavy quark mass M to satisfy NRQCD dispersion relations [56]. To study the finite-temperature modification of NRQCD propagators, an approximate choice of $a_s M$ such that $M \simeq 5$ GeV is sufficient.

There are many sources of systematic error in a lattice NRQCD calculation [58]. The three usual ones are effects of finite lattice spacing, finite volume and light quark vacuum polarization. Two more arise from the effective field theory nature: relativistic effects and radiative corrections to the couplings in the NRQCD expansion. Among these, finite volume effects are expected to be small for bottomonium since the physical size of bottomonium is small. Relativistic effects from the neglected higher order terms beyond $\mathcal{O}(v^4)$ are expected to be small as well since $v^2 \sim 0.1$. From experience in heavy quarkonium spectroscopy [56, 57], tadpole improvement is expected to reduce radiative corrections. The light quark masses used in this work are somewhat large but since the effects of the light quark vacuum polarization in heavy quarkonium physics is small, systematic effects from this are expected to be minor. The presence of a finite lattice spacing with the condition $Ma_s \sim 1$ is a well-known issue in lattice NRQCD, ruling out a continuum limit of NRQCD results, but at finite temperature this problem is no worse than at zero temperature. In all, the qualitative features of the finite temperature behaviour of bottomonium reported in this work are expected to remain valid even after the careful consideration of systematic errors.

4 Correlators

The starting point for the remainder of this paper is the high-precision euclidean correlators in the vector (Υ) and the pseudoscalar (η_b) channel, obtained by solving the NRQCD evolution equations. In Fig. 1 (top) we show these correlators, normalised with the value at $\tau = 0$ and on a logarithmic scale, for all temperatures available. Due to the use of NRQCD, there is no periodicity in the temporal direction. Combined with the large anisotropy, this implies that many temporal lattice points are available for the analysis, even at the highest temperature.

It is clear from the plots on the top that the temperature dependence is very mild. In order to make the temperature dependence visible, we show on the bottom the ratio of the high-temperature correlators with the one in the hadronic phase ($T/T_c = 0.42$, $N_\tau = 80$). We observe that the effect of increasing the temperature is monotonic and always below 3%. We remark here that the ratios depend on the sources used in the NRQCD evolution; the results shown here are obtained with point sources. Since potential model calculations typically

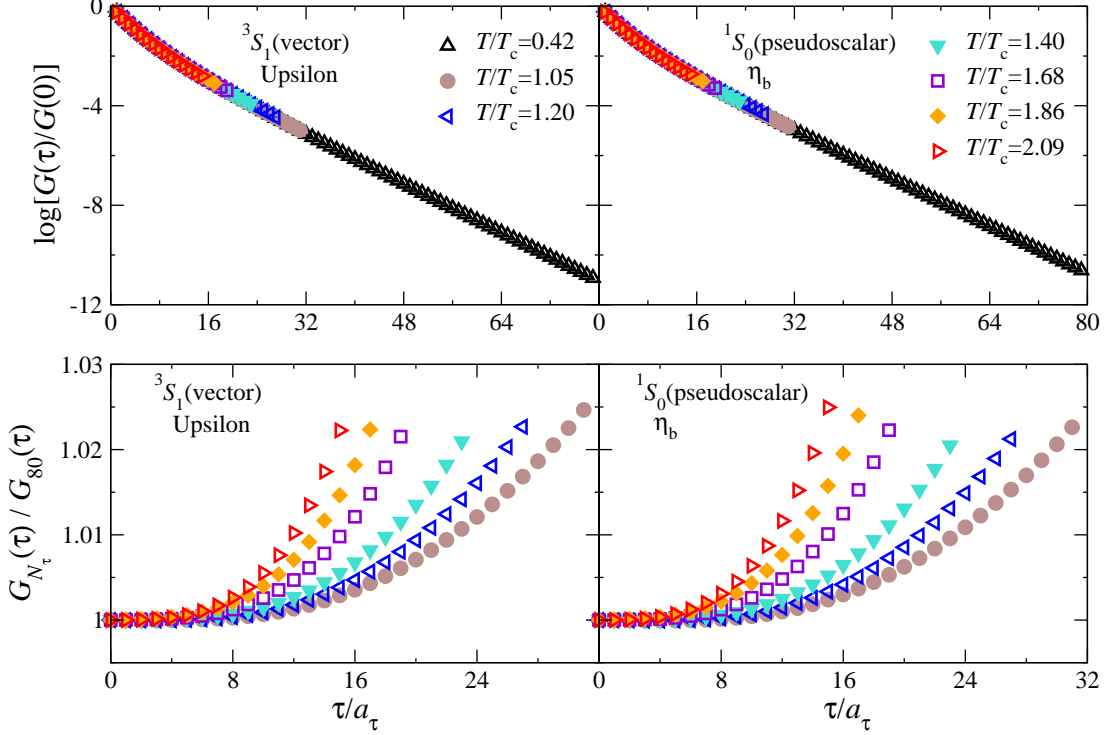


Figure 1: Euclidean correlation functions $G(\tau)$ as a function of the euclidean time in the vector (Υ) channel (left) and the pseudoscalar (η_b) channel (right), for all temperatures available, using point sources. At the top the correlators are normalised with the value at $\tau = 0$ and shown on a logarithmic scale, while on the bottom the high-temperature correlators are normalised with the correlator at the lowest temperature, $T/T_c = 0.42$ ($N_\tau = 80$). The errors are smaller than the symbols.

use point (delta function) sources as well, a comparison between potential model predictions and our NRQCD results should be possible.

In contrast to the relativistic case, the temperature dependence seen here does not arise from the thermal boundary conditions, but solely from the presence of the medium of gluons and light quarks at different temperatures. In terms of the spectral relation,

$$G(\tau) = \int \frac{d\omega}{2\pi} e^{-\omega\tau} \rho(\omega), \quad (4.1)$$

this is reflected in the temperature-independent kernel $e^{-\omega\tau}$. In the relativistic case, the temperature dependence of the kernel means a direct comparison between correlators at different temperatures is not straightforward. Often the kinematical temperature dependence is eliminated by using so-called reconstructed correlators, which requires the calculation of a spectral function at the lowest

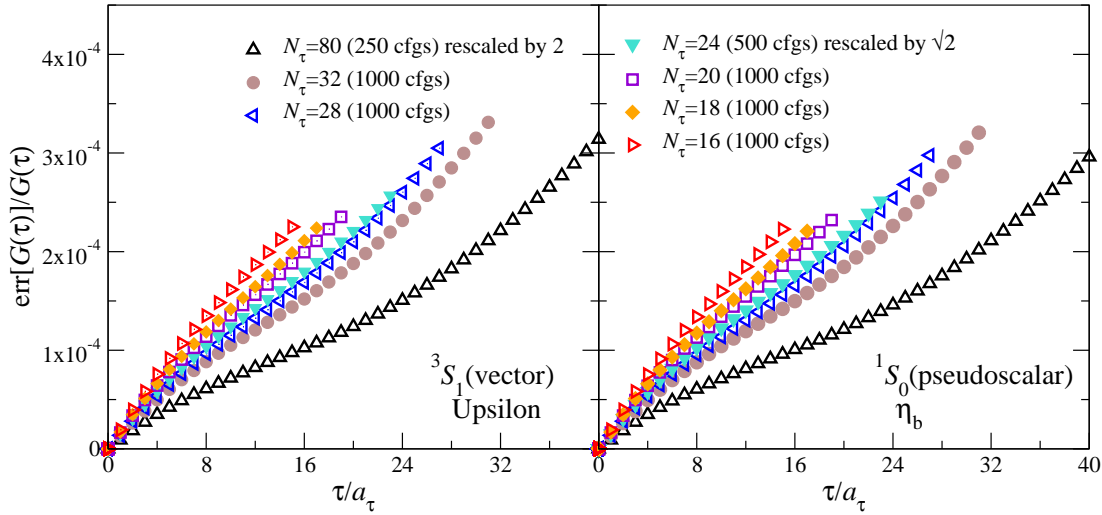


Figure 2: Relative error $\text{err}[G(\tau)]/G(\tau)$ as a function of euclidean time in the vector (left) and the pseudoscalar (right) channels. The data at $N_\tau = 80$ and 24 are rescaled to take into account the lower number of configurations.

available temperature [60]. This is not needed here and therefore the ratios in Fig. 1 (below) are a proper reflection of the presence of the temperature-dependent medium.

The statistical errors are small and not visible in the plots discussed above. To illustrate this, we show the statistical relative error, i.e., $\text{err}[G(\tau)]/G(\tau)$, as a function of euclidean time in Fig. 2. At all but two temperatures, there are 1000 configurations available. To take this into account, we rescaled the $N_\tau = 80$ data by a factor 2 (250 configurations) and the $N_\tau = 24$ data by a factor $\sqrt{2}$ (500 configurations). We then observe that the relative error is of the order of 10^{-4} and that it increases as the temperature of the quark-gluon plasma is increased, indicating larger thermal fluctuations in the hot phase.

From the data at the lowest temperature, we extract the masses of the ground states and the first excited states using standard exponential fits. The results are summarised in Table 2 and were already presented in Ref. [41].⁴ In NRQCD, all energies are determined only up to an additive constant, $E = E_0 + \Delta E$. Taking the $\Upsilon(1S)$ mass from the Particle Data Book [61] to set the scale, we find $E_0 = 8.57$ GeV.

⁴In Ref. [41] a temporal lattice spacing of $a_\tau^{-1} = 7.23$ GeV rather than 7.35 GeV was used, correcting this results in a small change in the mass predictions in the third column.

state	$a_\tau \Delta E$	Mass (MeV)	Exp. (MeV) [61]
$1^1S_0(\eta_b)$	0.118(1)	9438(8)	9390.9(2.8)
$2^1S_0(\eta_b(2S))$	0.197(2)	10019(15)	-
$1^3S_1(\Upsilon)$	0.121(1)	9460*	9460.30(26)
$2^3S_1(\Upsilon')$	0.198(2)	10026(15)	10023.26(31)
$1^1P_1(h_b)$	0.178(2)	9879(15)	$9898.3 \pm 1.1^{+1.0}_{-1.1}$ [62]
$1^3P_0(\chi_{b0})$	0.175(4)	9857(29)	9859.44(42)(31)
$1^3P_1(\chi_{b1})$	0.176(3)	9864(22)	9892.78(26)(31)
$1^3P_2(\chi_{b2})$	0.182(3)	9908(22)	9912.21(26)(31)

Table 2: Zero temperature bottomonium spectroscopy. The $1^3S_1(\Upsilon)$ state is used to set the scale. Here we concentrate on the Υ and η_b states.

5 Spectral functions

We extract spectral functions from the euclidean correlators presented above using the Maximum Entropy Method (MEM) [42]. A straightforward inversion of Eq. (4.1) is not possible, since euclidean correlators are determined numerically at a finite number of points, whereas spectral functions are in principle continuous functions of the energy ω . Using the ideas of Bayesian probability theory, one can construct the most probable spectral function by maximizing the conditional probability $P[\rho|DH]$, where D indicates the data and H some additional prior knowledge, encoded in a default model. In this section we present the results, while a discussion of the systematic uncertainties is given in the next section. We only consider spectral functions at zero spatial momentum.

The results for the spectral functions at the lowest temperature are given in Fig. 3. The vertical lines indicate the position of the ground state and first excited state from Table 2. We observe that the ground state appears as a very narrow peak in the spectral function, while the first excited state is broader and overlaps with structure at larger energy. The third feature, visible in the inset, is presumably a combination of higher excited states and lattice artefacts (see Appendix A).⁵ We note that quadruple precision is required for the MEM inversion, due to the large number of points ($N_\tau = 80$) and the exponential fall-off.

The main result of this paper is the spectral functions at the various temperatures, shown in Fig. 4 for the vector (Υ) channel (upper panel) and the pseudoscalar (η_b) channel (lower panel). Every panel contains two adjacent temperatures, from the coldest ($T/T_c = 0.42$) in the top left to the hottest ($T/T_c = 2.09$) in the bottom right. In each panel, the lower temperature is depicted with a

⁵Note in particular that it cannot be identified with the second excited state $\Upsilon(3S)$, with a mass of 10.3552 GeV [61].

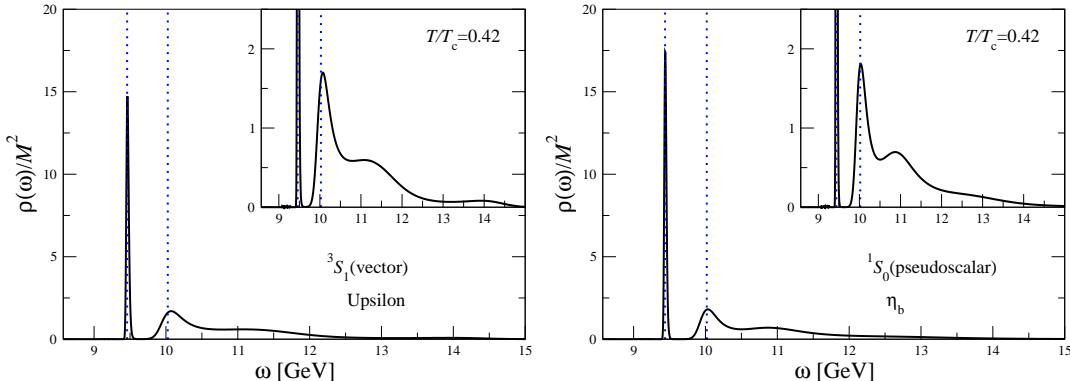


Figure 3: Spectral functions $\rho(\omega)$, normalised with the heavy quark mass, as a function of energy at the lowest temperature in the vector (Υ) and the pseudoscalar (η_b) channels. The vertical lines indicate the positions of the ground and first excited state obtained via standard exponential fits. The insets show a close-up.

dashed line and the higher one with a solid line. As the temperature is increased, we observe that the ground state peak remains visible, even though it broadens and reduces in height. The excited states become less pronounced as the temperature increases and are no longer discernible as a separate peak between $1.4 \lesssim T/T_c \lesssim 1.68$.⁶ This can be interpreted as the survival of the $1S$ states, but a melting or suppression of the excited states. From the analysis in Sec. 6, we note here that we consider the results for the spectral functions to be robust for all temperatures, with the exception of the two highest temperatures where uncertainties due to the limited statistics and euclidean time range remain.

We note that the area under the curve is determined by the source⁷ at $\tau = 0$ and the spectral relation,

$$\int \frac{d\omega}{2\pi} \rho(\omega, \mathbf{p} = \mathbf{0}) = \int d^3x G(\tau = 0, \mathbf{x}) = \int d^3x S(\mathbf{x}), \quad (5.1)$$

and is independent of the temperature.

The peak position E and width Γ of the ground states can be extracted by fitting the peaks to a Gaussian function. We fit to the left side of the peak, to avoid contamination from the features at larger ω . In Fig. 5 (top panel) we show the temperature dependence of the mass shift ΔE , normalised with the heavy quark mass. Recall that in NRQCD only energy differences can be determined, and that the total energy is $E = E_0 + \Delta E$, where $E_0 = 8.57$ GeV in

⁶We also note that the second peak immediately above T_c is presumably a combination of the first excited state and other features.

⁷The point source is defined to be unity for each of the upper two-component spinor indices as well as for each of the colour indices.

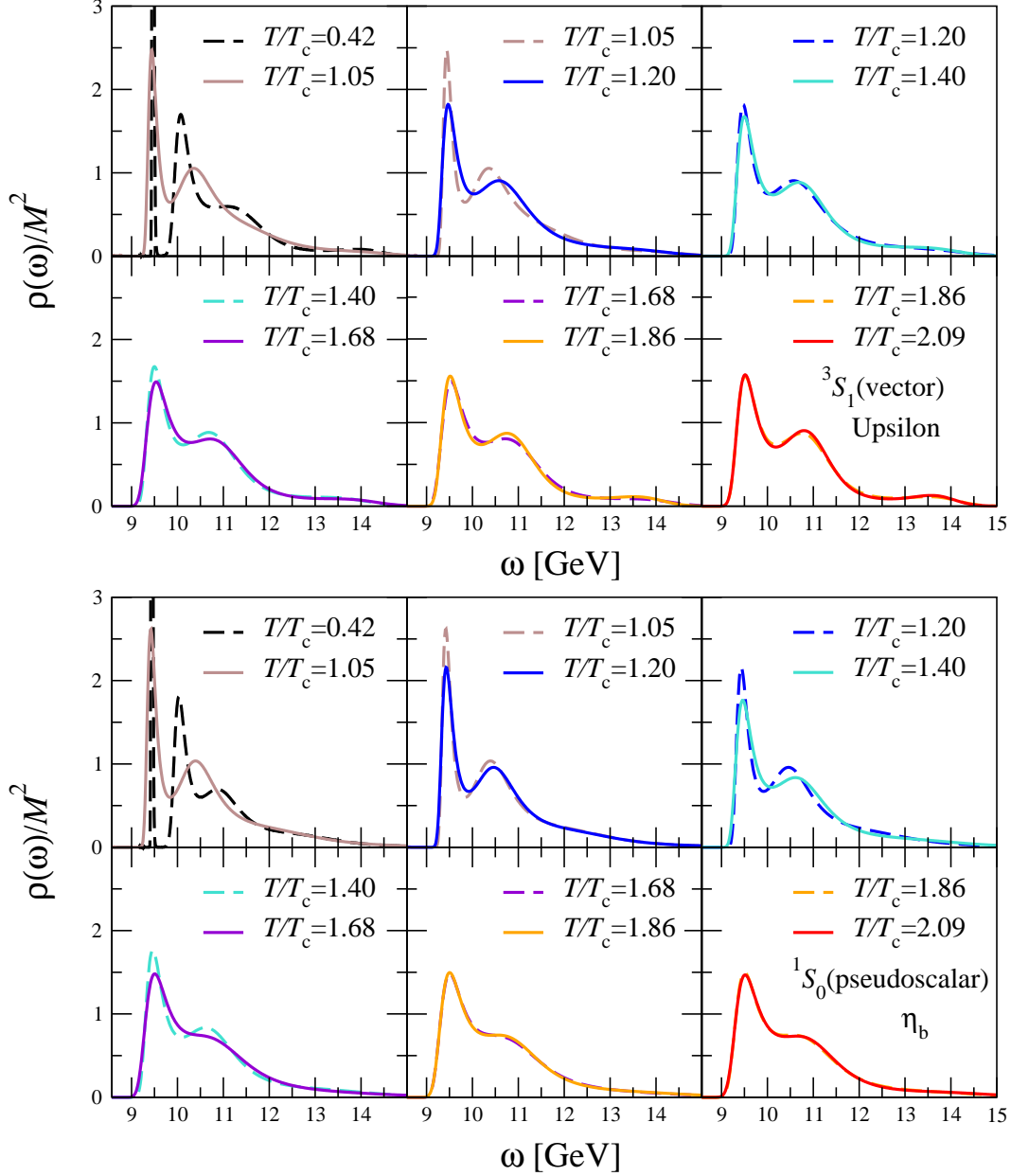


Figure 4: Spectral functions $\rho(\omega)$, normalised with the heavy quark mass, in the vector (Υ) channel (upper panel) and in the pseudoscalar (η_b) channel (lower panel) for all temperature available. The subpanels are ordered from cold (top left) to hot (bottom right). Every subpanel contains two adjacent temperatures to facilitate the comparison.

our case. The temperature dependence of the width is shown in Fig. 5 (bottom panel). Note that the width is normalised with the temperature. The error bars

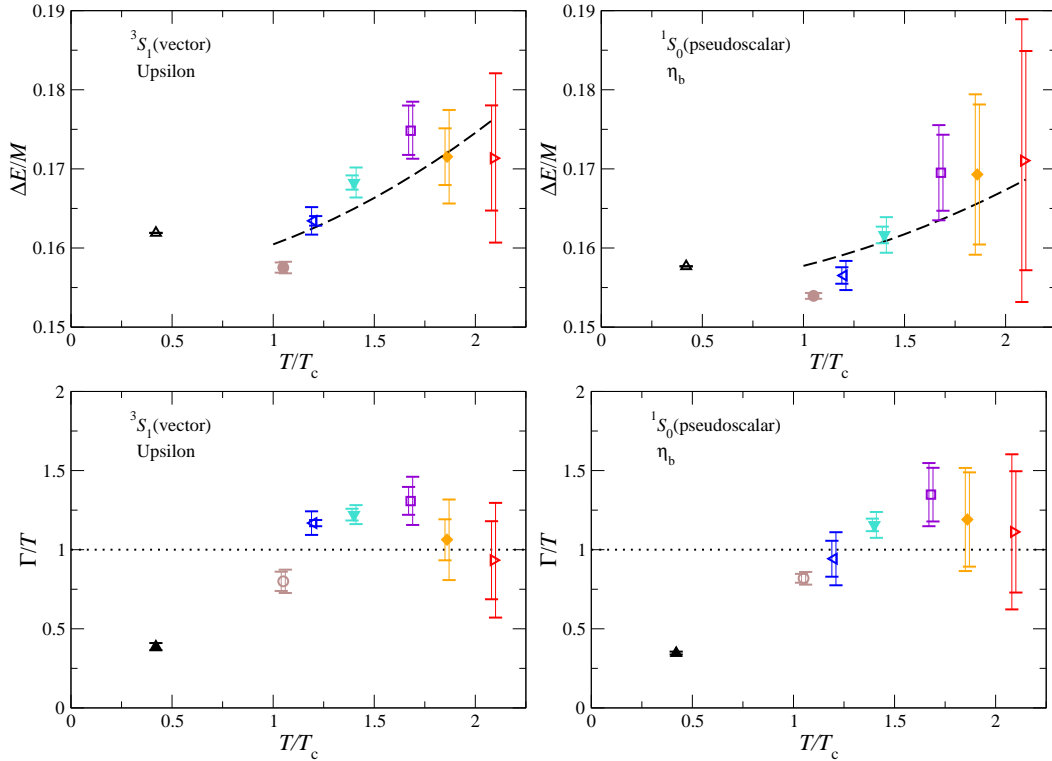


Figure 5: Position of the ground state peak ΔE , normalised with the heavy quark mass (upper panels), and the upper limit on the width of the ground state peak, normalised with the temperature (lower panels), as a function of T/T_c in the vector (Υ) and the pseudoscalar (η_b) channels. The error bars denote the systematic uncertainty with the left error bars representing the error from the finiteness of the last time in the fitting window, τ_2 , and the right error bar representing the error from the finite statistics (see Sec. 6). The lines in the upper plots indicate expected analytical behaviour assuming weak coupling above T_c .

indicate systematic uncertainties in extracting the peak position and width from the peaked structure. In Sec. 6 these uncertainties are discussed in detail. Based on this discussion we conclude conservatively that the width shown in Fig. 5 is better interpreted as an upper bound, rather than the width itself.

To see whether these results are reasonable, we now take them at face value and contrast them with analytic predictions derived assuming a weakly coupled plasma. According to Ref. [31], the thermal contribution to the width is given, at leading order in the weak coupling and large mass expansion, by

$$\frac{\Gamma}{T} = \frac{1156}{81} \alpha_s^3 \simeq 14.27 \alpha_s^3, \quad (5.2)$$

i.e., the width increases linearly with the temperature.⁸ If we take as an estimate from our results that $\Gamma/T \sim 1$, we find that this corresponds to $\alpha_s \sim 0.4$, which is a reasonable result. In the same spirit the thermal mass shift is given in Ref. [31] by

$$\delta E_{\text{thermal}} = \frac{17\pi}{9} \alpha_s \frac{T^2}{M} \simeq 5.93 \alpha_s \frac{T^2}{M}. \quad (5.3)$$

In these simulations we have $T_c \sim 220$ MeV, $M \sim 5$ GeV. Taking these values together with $\alpha_s \sim 0.4$ as determined above, Eq. (5.3) becomes

$$\frac{\delta E_{\text{thermal}}}{M} = 5.93 \alpha_s \left(\frac{T_c}{M}\right)^2 \left(\frac{T}{T_c}\right)^2 \sim 0.0046 \left(\frac{T}{T_c}\right)^2. \quad (5.4)$$

In order to contrast our results with this analytical prediction, we have compared the temperature dependence of the peak positions to the simple expression

$$\frac{\Delta E}{M} = c + 0.0046 \left(\frac{T}{T_c}\right)^2, \quad (5.5)$$

where c is a free parameter. This is shown by the dashed lines in Fig. 5 (top panel). While we are not in a position to confirm or rule out the quadratic temperature dependence due to the systematic uncertainties in the MEM analysis and the fitting of the ground state peaks, we note that our results are not inconsistent with this. In particular, the absolute scale of temperature variation seems to be of the correct order. We also note that the mass just above T_c is reduced with respect to the low temperature one.

6 Systematics and uncertainties

In order to assess the robustness of the results presented above, in this section we discuss the main systematic uncertainties, namely the dependence on the default model, the choice of ω_{\min} , the number of configurations and the euclidean time window, and explain the error estimates of the previous section. We only show results for the vector channel; the ones in the pseudoscalar channel are similar.

Default model

The MEM procedure includes a “default model” $m(\omega)$ which is used to define the entropy term,

$$S = \int_{\omega_{\min}}^{\omega_{\max}} \frac{d\omega}{2\pi} \left[\rho(\omega) - m(\omega) - \rho(\omega) \ln \frac{\rho(\omega)}{m(\omega)} \right], \quad (6.1)$$

⁸A linearly rising width with temperature was also predicted in Ref. [25].

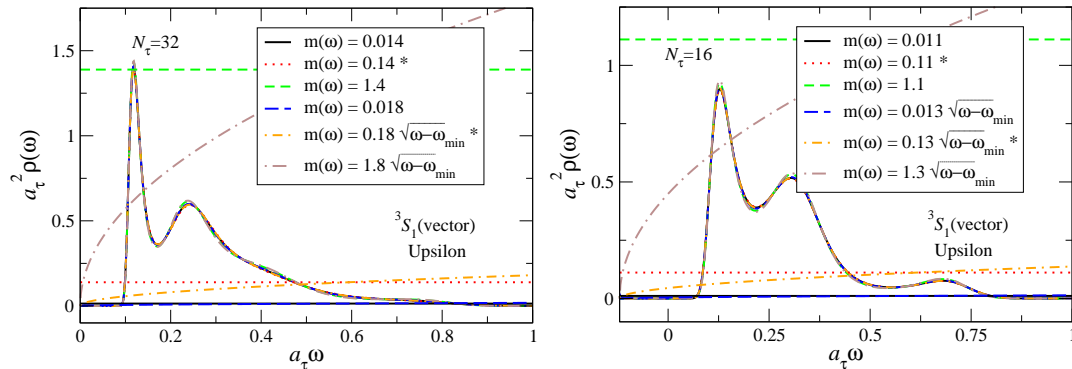


Figure 6: Dependence of the spectral function on the default model chosen in the MEM analysis for $N_\tau = 32$ (left) and 16 (right), in the vector channel. The default models favoured by the χ^2 minimization are denoted with a $*$.

in the MEM approach. It is expected that with poor data the spectral function will resemble the default model, since this minimises the entropy, but that with precise data the choice of default model becomes irrelevant. The usual procedure is to choose a default model which has the same functional form as the (continuum) free spectral function in the channel under consideration. For the nonrelativistic S wave, this is $m(\omega) = m_0\sqrt{\omega}$, see Eq. (A.4). An alternative is to use a constant default model, $m(\omega) = m_0$. The constants m_0 can be set by minimising the χ^2 between the data and the correlation function defined from the default model,

$$G_{\text{def}}(\tau) = \int_{\omega_{\text{min}}}^{\omega_{\text{max}}} \frac{d\omega}{2\pi} e^{-\omega\tau} m(\omega).$$

To illustrate the absence of default model dependence in our analysis, we show here results for the following six default models:

- $m(\omega) = m_0\sqrt{\omega}$, with $m_0/m_0^* = 0.1, 1, 10$,
- $m(\omega) = m_0$, with $m_0/m_0^* = 0.1, 1, 10$,

where in both cases m_0^* is determined by minimizing χ^2 as described above.

In Fig. 6 we show the resulting six spectral functions, as well as the six default models used, at $T/T_c = 1.05$ and 2.09. We observe that the spectral functions do not resemble the default models and that there is almost no variation in the spectral functions, even with default models varying over two orders of magnitude. We conclude that there is no significant default model dependence in this analysis, even at the highest temperature.

N_τ	N_ω	Υ (vector channel)		η_b (pseudoscalar channel)	
		$a_\tau\omega_{\min}$	$a_\tau\omega_{\max}$	$a_\tau\omega_{\min}$	$a_\tau\omega_{\max}$
80	4000	0.00	2.00	0.00	2.00
32	1000	0.00	1.50	0.00	2.00
28	1000	-0.04	1.46	-0.08	1.92
24	1000	-0.10	1.40	-0.10	1.90
20	1000	-0.10	1.40	-0.10	1.90
18	1000	-0.10	1.40	-0.10	1.90
16	1000	-0.12	0.88	-0.12	1.88

Table 3: Details of the parameters used in the MEM analysis. Note that $\Delta\omega = (\omega_{\max} - \omega_{\min})/N_\omega$, and that $a_\tau\omega = 0$ and 2 correspond to 8.57 GeV and 23.3 GeV respectively.

Energy window

Since in NRQCD the heavy quark mass scale is removed, the additive normalization of the energy scale has to be determined by comparing to a physical state. For this reason, setting the lower boundary $\omega_{\min} = 0$ in the spectral relation (4.1) is not a priori justified and it might be necessary to allow for the possibility of negative energies ($\omega_{\min} < 0$) in the energy integral. Indeed, in the high temperature cases we noticed that when $\omega_{\min} \sim 0$, the MEM spectral functions have a spike in the lowest-energy bin, which we interpret as an unphysical effect. Reducing ω_{\min} to negative values reduces this spike until it is essentially absent when $a_\tau\omega_{\min} \sim -0.10$. At the lower temperatures ($N_\tau = 80, 32$), no spikes were observed with $\omega_{\min} = 0$. In Table 3 we list the parameters used in the MEM analysis. N_ω denotes the number of points in which the energy interval $\omega_{\max} - \omega_{\min}$ is divided.

Number of configurations

In Fig. 7 we illustrate how the position and width of the ground state peak depend on the number of configurations used in the MEM analysis. For clarity, we only show results for a selection of N_τ values. At each temperature, we divide the total number of configurations (1000) into 20 groups of 50, 10 groups of 100, 5 groups of 200, 3 groups of 333, and 2 groups of 500, and compute the spectral function for each of them. The resulting peak position and width are shown as a function of $1/\sqrt{N_{\text{cfgs}}}$. At the lower temperatures ($N_\tau = 32, 28, 24$) we observe that both are essentially independent of the number of configurations used and the results are stable. At the higher temperature ($N_\tau = 20$) there is a larger spread for the low-statistics results, but the average results are again quite stable, with at most only a slight decrease in the width and mass as the statistics are increased. It is

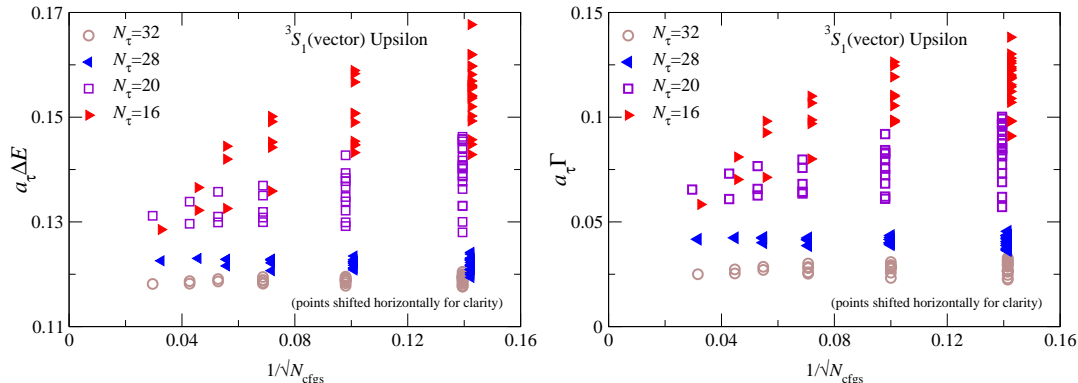


Figure 7: Dependence of the position (ΔE) and width (Γ) of the ground state peak extracted from the spectral function on the number N_{cfgs} of configurations used, in the vector channel.

only at the highest temperatures ($N_\tau = 18, 16$) that there is a clear decrease in the position and width with increased statistics. We conclude that the statistical error due to the finiteness of the ensemble does not prevent us from determining the ground state mass and width, at all but the highest two temperatures.

To translate the dependence on the number of configurations into an uncertainty in the position and width of the ground state, we proceed as follows. The central value is taken from the analysis with 1000 configurations. The statistical error due to the finite number of configurations is defined by taking the difference between the central value and the value obtained with 500 configurations which is furthest from the central value. This statistical error is shown as the right-hand error bar in Fig. 5.

Euclidean time window

The euclidean time window included in the MEM analysis is $\tau_1 \leq \tau \leq \tau_2$, with the initial time equal to the first time slice, i.e. $\tau_1 = a_\tau$.⁹ In Fig. 8 we show the dependence of the constructed spectral functions on τ_2 for $N_\tau = 20$ (left) and $N_\tau = 16$ (right), varying τ_2 from a small value up to $N_\tau - 1$. Both cases are at high temperature, $T/T_c = 1.68$ and 2.09 respectively. We observe that at $N_\tau = 20$ the result is stable and the limitation of having only a finite number of points in the temporal direction does not appear to be a problem. At the highest temperature, on the other hand, we note that the results have not yet stabilised, so that the uncertainty in constructing the spectral function is larger.

In order to quantify this, we have determined the τ_2 dependence of the position and peak of the ground state at all temperatures. The result is shown in

⁹Varying τ_1 within reason did not have a significant effect.

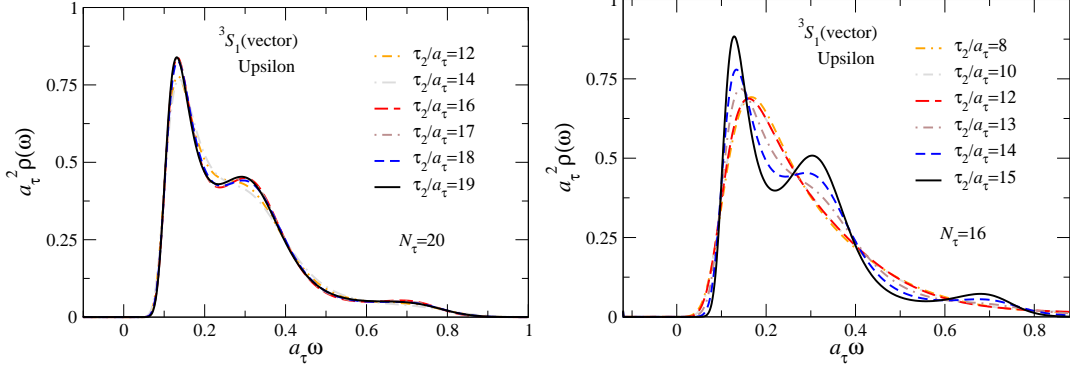


Figure 8: Dependence of spectral functions on the euclidean time window $a_\tau = \tau_1 \leq \tau \leq \tau_2$, for several values of τ_2 for $N_\tau = 20$ (left) and 16 (right), in the vector channel.

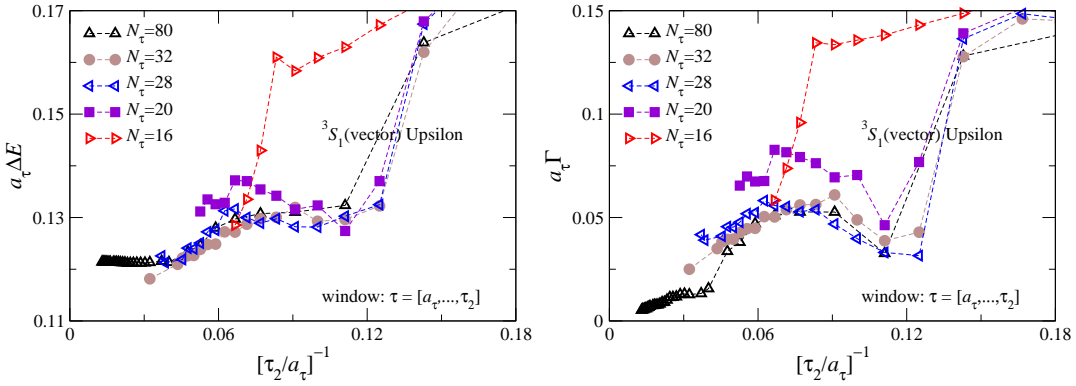


Figure 9: Dependence of the position (ΔE , left) and width (Γ , right) of the ground state peak extracted from the spectral function on the euclidean time window $a_\tau = \tau_1 \leq \tau \leq \tau_2$ used in the MEM analysis, in the vector channel.

Fig. 9 for a selection of N_τ values. For the lowest temperature ($N_\tau = 80$), we observe that ΔE is stable and consistent with the result from the standard fits directly to the euclidean correlator. Moreover, there is evidence that the width Γ decreases towards zero as τ_2 increases. The position and width at $N_\tau = 32, 28$, or $T/T_c = 1.05, 1.20$, appear to behave as in the hadronic phase, except for a possible flattening out of the width for $N_\tau = 28$ at large τ_2 . A similar behaviour is found for $N_\tau = 24$, with a clearer tendency for both the position and width to flatten out at large τ_2 . On the other hand, at $N_\tau = 20$ both position and width are consistently above their low-temperature values, and may reach a plateau for large τ_2 , consistent with Fig. 8. For $N_\tau = 18$ and 16, no stability is seen. For $N_\tau = 16$, it follows from Fig. 8 that when τ_2 is too small, the ground state and

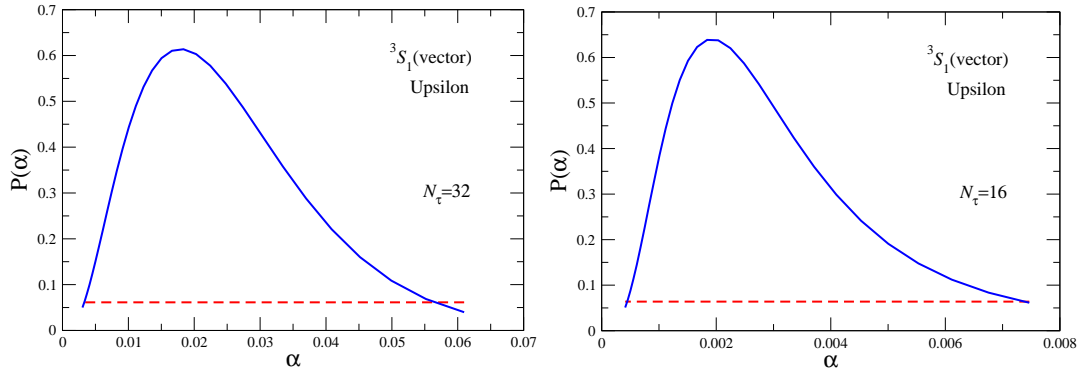


Figure 10: The probability $P(\alpha)$ used in Bryan's approach for $N_\tau = 32$ (left) and 16 (right). The horizontal lines indicate the interval used in the integral in Eq. (6.3).

features at larger energies overlap and therefore the ground state peak cannot be resolved. At $\tau_2/a_\tau \gtrsim 13$, two structures become visible, which explains the rapid drop of the position and peak. We conclude therefore that at most temperatures above T_c the position and width of the groundstate peak appear to be stable, except at the highest two temperatures where substantial dependence on τ_2 remains.

To translate the finiteness of τ_2 into a systematic uncertainty on the position and width of the ground state, we adopt the following procedure. The central value is taken from the analysis with $\tau_2 = N_\tau - 1$. The systematic error due to a finite τ_2 is defined by taking the difference between the central value and the value obtained with $\tau_2 = N_\tau - 2$. This systematic error is shown as the left-hand error bar in Fig. 5.

Bryan's approach

In the MEM approach, Bayes' theorem implies that the entropy term S is balanced against the usual maximum likelihood χ^2 . The function Q to be maximized is

$$Q = \alpha S - \chi^2, \quad (6.2)$$

where S is defined in Eq. (6.1) and α is a normalisation constant which is to be determined. In Bryan's approach [52] the spectral function $\rho_\alpha(\omega)$ is calculated for each value of α and the final spectral function is obtained by performing the convolution integral,

$$\rho_{\text{final}}(\omega) = \int d\alpha P(\alpha) \rho_\alpha(\omega). \quad (6.3)$$

Here $P(\alpha)$ is the probability that α is chosen correctly.

In Fig. 10, the probability $P(\alpha)$ is plotted for the Υ channel for $N_\tau = 32$ and 16. In practice, the limits in the integral in Eq. (6.3) are taken such that $P(\alpha)$ is greater than some fraction of its maximum value P_{\max} . In this case, we use the interval defined as $P(\alpha)/P_{\max} > 0.1$ and the resulting interval is shown in Fig. 10 by the horizontal lines. In all cases we find that the probability is well defined with a clear maximum.

7 Conclusion

In this paper we analysed lattice QCD results for S wave bottomonium correlators (in the Υ and η_b channels). The heavy quarks are treated with NRQCD and propagate through a two-flavour quark-gluon medium at seven temperatures between $0.4T_c$ and $2.1T_c$. Highly anisotropic lattices, with $a_s/a_\tau = 6$, are used to maximise the number of time slices available for the analysis. Spectral functions are constructed with the help of the maximum entropy method.

The use of NRQCD has a number of advantages compared to relativistic quark dynamics. Since the presence of a nonzero temperature is not imposed as a thermal boundary condition, twice as many euclidean time points are available for the analysis compared to the relativistic case (at the same temperature and lattice spacing). More importantly, the spectral relation simplifies considerably, removing the problem with the so-called constant contribution in the correlator. Physically, it implies that all temperature dependence is due to the presence of the light-quark-gluon system.

Our main results are spectral functions for the S waves, in the vector (Υ) and pseudoscalar (η_b) channels. Our results suggest that the ground state survives up to the highest temperature we consider, whereas the excited states are suppressed and no longer visible at temperatures above $1.4T_c$. We have extracted the position and width of the ground state peaks and found them to be consistent with analytical results obtained within the EFT framework, at leading order in the large mass expansion.

Systematic uncertainties have been studied in some detail. For all temperatures, we found no dependence on the default model used in the MEM analysis. The position and width of the ground state peaks were shown to be stable as the number of configurations is increased, for all except the highest temperatures. Perhaps the biggest uncertainty comes from the finite number of euclidean time points, but our analysis suggests that the peak position and width can still be reliably determined for temperatures up to $1.7T_c$.

We hope that our results will be useful for further EFT and potential model studies. After constructing a temperature-dependent potential, one usually computes spectral functions and the corresponding euclidean correlators. It would be interesting to compare the outcome of such an exercise with our nonperturbatively determined correlators. This would in particular be applicable to ratios

of finite-temperature correlators with the zero-temperature one, as in Fig. 1, to cancel normalization factors and focus on the temperature dependence.

Finally, we hope that our results will contribute to a further understanding of the recent experimental results for bottomonium in heavy ion collisions at the LHC and RHIC.

Acknowledgments

We thank Mikko Laine for discussion and clarification. CA, GA and MPL thank Trinity College Dublin and the National University of Ireland Maynooth for hospitality. We acknowledge the support and infrastructure provided by the Trinity Centre for High Performance Computing and the IITAC project funded by the HEA under the Program for Research in Third Level Institutes (PRTLII) co-funded by the Irish Government and the European Union. The work of CA and GA is carried as part of the UKQCD collaboration and the DiRAC Facility jointly funded by STFC, the Large Facilities Capital Fund of BIS and Swansea University. GA and CA are supported by STFC. SK is grateful to STFC for a Visiting Researcher Grant and supported by the National Research Foundation of Korea grant funded by the Korea government (MEST) No. 2011-0026688. SR is supported by the Research Executive Agency (REA) of the European Union under Grant Agreement number PITN-GA-2009-238353 (ITN STRONGnet) and the Science Foundation Ireland, grant no. 11/RFP.1/PHY/3201. DKS is supported in part by US Department of Energy contract DE-AC02-06CH11357. JIS is supported by Science Foundation Ireland grant 08-RFP-PHY1462.

A Noninteracting lattice spectral functions

In order to understand the effect of lattice artefacts, it is useful to construct lattice spectral functions in the absence of interactions, adapting the approach of Refs. [63,64] to lattice NRQCD.

Let us start with free quarks in continuum NRQCD with energy $E_{\mathbf{p}} = \mathbf{p}^2/2M$. The correlators for the S and P waves at zero spatial momentum are then of the form [27]

$$G_S(\tau) = 2N_c \int \frac{d^3p}{(2\pi)^3} e^{-2E_{\mathbf{p}}\tau} = \frac{N_c}{4\pi^{3/2}} \left(\frac{M}{\tau}\right)^{3/2}, \quad (\text{A.1})$$

$$G_P(\tau) = 2N_c \int \frac{d^3p}{(2\pi)^3} \mathbf{p}^2 e^{-2E_{\mathbf{p}}\tau} = \frac{3N_c}{8\pi^{3/2}} \left(\frac{M}{\tau}\right)^{5/2}, \quad (\text{A.2})$$

where in the explicit evaluation we did not include an ultraviolet cutoff, since the integrals are finite for nonzero τ .

This is easily expressed in terms of spectral densities, using

$$G(\tau) = \int_{\omega_{\min}}^{\omega_{\max}} \frac{d\omega}{2\pi} e^{-\omega\tau} \rho(\omega), \quad (\text{A.3})$$

yielding

$$\rho_S(\omega) = 4\pi N_c \int \frac{d^3p}{(2\pi)^3} \delta(\omega - 2E_{\mathbf{p}}) = \frac{N_c}{\pi} M^{3/2} \omega^{1/2} \Theta(\omega), \quad (\text{A.4})$$

$$\rho_P(\omega) = 4\pi N_c \int \frac{d^3p}{(2\pi)^3} \mathbf{p}^2 \delta(\omega - 2E_{\mathbf{p}}) = \frac{N_c}{\pi} M^{5/2} \omega^{3/2} \Theta(\omega). \quad (\text{A.5})$$

Note that the minimal energy $\omega_{\min} = 0$ corresponds to twice the heavy quark mass, due to the nonrelativistic approximation, $\sqrt{\mathbf{p}^2 + M^2} \approx M + E_{\mathbf{p}}$. In the presence of a momentum cutoff $|\mathbf{p}| < \Lambda$, the maximum energy is finite and given by $\omega_{\max} = \Lambda^2/M$. Note also that there is no temperature dependence in the absence of interactions. All temperature effects enter via the propagation through the quark-gluon system.

These results can easily be adapted to the lattice [63, 64], taking into account the lattice dispersion relation and the finite momentum integration over the first Brillouin zone. At lowest order in (unimproved) NRQCD, the dispersion relation is

$$a_\tau E_{\mathbf{p}} = -\log \left(1 - \frac{\hat{\mathbf{p}}^2}{2\xi \hat{M}} \right), \quad (\text{A.6})$$

where $\hat{M} = a_s M$, $\xi = a_s/a_\tau$, and

$$\hat{\mathbf{p}}^2 = 4 \sum_{i=1}^3 \sin^2 \left(\frac{p_i}{2} \right), \quad p_i = \frac{2\pi n_i}{N_s}, \quad n_i = -\frac{N_s}{2} + 1, \dots, \frac{N_s}{2}, \quad (\text{A.7})$$

with N_s the number of sites in a spatial direction. The lattice spectral functions then take the form

$$\rho_S(\omega) = \frac{4\pi N_c}{N_s^3} \sum_{\mathbf{p}} \delta(\omega - 2E_{\mathbf{p}}), \quad (\text{A.8})$$

$$\rho_P(\omega) = \frac{4\pi N_c}{N_s^3} \sum_{\mathbf{p}} \hat{\mathbf{p}}^2 \delta(\omega - 2E_{\mathbf{p}}), \quad (\text{A.9})$$

where the sums go over all momenta in the first Brillouin zone. Evaluating these numerically, as in Refs. [63, 64], yields the spectral functions shown in Fig. 11. Here N_s is taken large enough to be in the spatial thermodynamic limit, while there is no dependence on N_τ . Improving the dispersion relation will give better agreement between lattice and continuum results at small ω . The cusps result from reaching the edge of the Brillouin zone in the (1,0,0) or

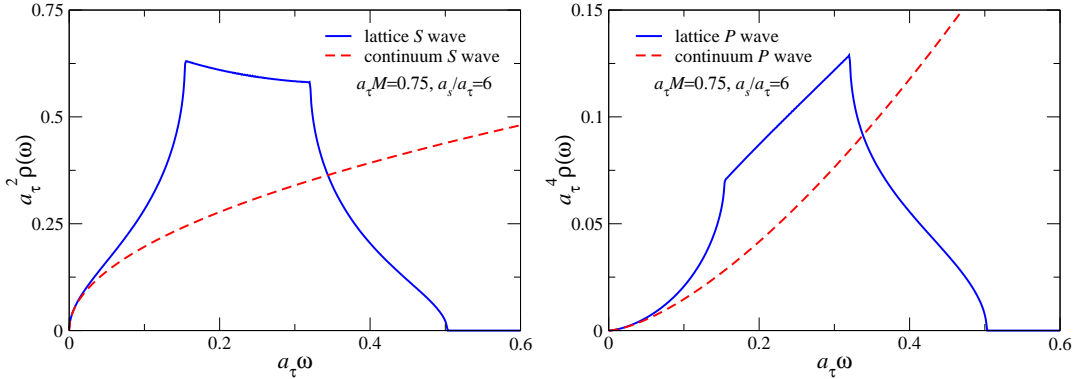


Figure 11: Lattice spectral functions, in units of the temporal lattice spacing a_τ , as a function of $a_\tau\omega$, for S waves (left) and P waves (right) in anisotropic lattice NRQCD at lowest order, ignoring interactions, using $\xi \equiv a_s/a_\tau = 6$ and $a_\tau M = 0.75$. The dashed lines indicate the continuum spectral functions in the absence of a cutoff.

(1,1,0) direction (+ permutations). The maximal energy is determined by the maximal lattice momentum in the (1,1,1) direction, namely $\hat{\mathbf{p}}^2 = 12$, and equals $a_\tau\omega_{\text{max}}^{\text{lat}} = 0.503$ for the parameters used here. Comparing these results with those for free relativistic quarks [63, 64], we conclude that the main difference is the temperature (or N_τ) independence.

References

- [1] T. Matsui and H. Satz, Phys. Lett. B **178** (1986) 416.
- [2] R. Arnaldi [NA60 Collaboration], Nucl. Phys. A **830** (2009) 345C [arXiv:0907.5004 [nucl-ex]].
- [3] A. Adare *et al.* [PHENIX Collaboration], Phys. Rev. Lett. **101** (2008) 122301 [arXiv:0801.0220 [nucl-ex]].
- [4] H. Satz, Nucl. Phys. A **783** (2007) 249 [arXiv:hep-ph/0609197].
- [5] R. Rapp, D. Blaschke and P. Crochet, Prog. Part. Nucl. Phys. **65** (2010) 209 [arXiv:0807.2470 [hep-ph]].
- [6] S. Chatrchyan *et al.* [CMS Collaboration], Phys. Rev. Lett. **107** (2011) 052302.
- [7] R. Reed [STAR Collaboration], arXiv:1109.3891 [nucl-ex].
- [8] M. Strickland, arXiv:1106.2571 [hep-ph].

- [9] F. Brezinski, G. Wolschin, arXiv:1109.0211 [hep-ph].
- [10] A. Mócsy and P. Petreczky, Phys. Rev. D **77** (2008) 014501 [arXiv:0705.2559 [hep-ph]].
- [11] A. Mócsy, P. Petreczky, Phys. Rev. Lett. **99** (2007) 211602 [arXiv:0706.2183 [hep-ph]].
- [12] T. Umeda, K. Nomura, H. Matsufuru, Eur. Phys. J. **C39S1** (2005) 9-26 [hep-lat/0211003].
- [13] M. Asakawa, T. Hatsuda, Phys. Rev. Lett. **92** (2004) 012001 [hep-lat/0308034].
- [14] S. Datta, F. Karsch, P. Petreczky, I. Wetzorke, Phys. Rev. **D69** (2004) 094507 [hep-lat/0312037].
- [15] A. Jakovác, P. Petreczky, K. Petrov and A. Velytsky, Phys. Rev. D **75** (2007) 014506 [arXiv:hep-lat/0611017].
- [16] G. Aarts, C. Allton, M. B. Oktay, M. Peardon and J. I. Skullerud, Phys. Rev. D **76** (2007) 094513 [arXiv:0705.2198 [hep-lat]].
- [17] M. B. Oktay and J. I. Skullerud, arXiv:1005.1209 [hep-lat].
- [18] H. -T. Ding, A. Francis, O. Kaczmarek, H. Satz, F. Karsch, W. Söldner, PoS **LATTICE2010** (2010) 180 [arXiv:1011.0695 [hep-lat]].
- [19] H. Ohno *et al.* [WHOT-QCD Collaboration], arXiv:1104.3384 [hep-lat].
- [20] J. Noronha, A. Dumitru, Phys. Rev. Lett. **103** (2009) 152304 [arXiv:0907.3062 [hep-ph]].
- [21] H. R. Grigoryan, P. M. Hohler, M. A. Stephanov, Phys. Rev. **D82** (2010) 026005 [arXiv:1003.1138 [hep-ph]].
- [22] H. R. Grigoryan, Y. V. Kovchegov, Nucl. Phys. **B852** (2011) 1-38 [arXiv:1105.2300 [hep-th]].
- [23] I. M. Narodetskiy, Y. A. Simonov, A. I. Veselov, arXiv:1102.5453 [hep-ph].
- [24] K. Marasinghe, K. Tuchin, arXiv:1103.1329 [hep-ph].
- [25] M. Laine, O. Philipsen, P. Romatschke and M. Tassler, JHEP **0703** (2007) 054 [arXiv:hep-ph/0611300].
- [26] M. Laine, JHEP **0705** (2007) 028 [arXiv:0704.1720 [hep-ph]].

- [27] Y. Burnier, M. Laine and M. Vepsäläinen, JHEP **0801** (2008) 043 [arXiv:0711.1743 [hep-ph]].
- [28] M. Laine, Nucl. Phys. A **820** (2009) 25C [arXiv:0810.1112 [hep-ph]].
- [29] M. Laine, arXiv:1108.5965 [hep-ph].
- [30] N. Brambilla, J. Ghiglieri, A. Vairo and P. Petreczky, Phys. Rev. D **78** (2008) 014017 [arXiv:0804.0993 [hep-ph]].
- [31] N. Brambilla, M. A. Escobedo, J. Ghiglieri, J. Soto, A. Vairo, JHEP **1009** (2010) 038 [arXiv:1007.4156 [hep-ph]].
- [32] N. Brambilla, J. Ghiglieri, P. Petreczky, A. Vairo, Phys. Rev. **D82** (2010) 074019 [arXiv:1007.5172 [hep-ph]].
- [33] N. Brambilla, M. A. Escobedo, J. Ghiglieri, A. Vairo, JHEP **1107** (2011) 096 [arXiv:1105.4807 [hep-ph]].
- [34] A. Beraudo, J. P. Blaizot and C. Ratti, Nucl. Phys. A **806** (2008) 312 [arXiv:0712.4394 [nucl-th]].
- [35] A. Beraudo, J. P. Blaizot, P. Faccioli and G. Garberoglio, Nucl. Phys. A **846** (2010) 104 [arXiv:1005.1245 [hep-ph]].
- [36] P. Petreczky, C. Miao, A. Mócsy, Nucl. Phys. **A855** (2011) 125-132 [arXiv:1012.4433 [hep-ph]].
- [37] M. Margotta, K. McCarty, C. McGahan, M. Strickland, D. Yager-Elorriaga, Phys. Rev. **D83** (2011) 105019 [arXiv:1101.4651 [hep-ph]].
- [38] A. Rothkopf, T. Hatsuda, S. Sasaki, PoS **LAT2009** (2009) 162 [arXiv:0910.2321 [hep-lat]].
- [39] A. Rothkopf, T. Hatsuda, S. Sasaki, arXiv:1108.1579 [hep-lat].
- [40] J. Fingberg, Phys. Lett. B **424** (1998) 343 [arXiv:hep-lat/9707012].
- [41] G. Aarts, S. Kim, M. P. Lombardo, M. B. Oktay, S. M. Ryan, D. K. Sinclair, J. -I. Skullerud, Phys. Rev. Lett. **106** (2011) 061602 [arXiv:1010.3725 [hep-lat]].
- [42] M. Asakawa, T. Hatsuda, Y. Nakahara, Prog. Part. Nucl. Phys. **46** (2001) 459-508 [hep-lat/0011040].
- [43] G. Aarts, C. Allton, S. Kim, M. P. Lombardo, M. B. Oktay, S. M. Ryan, D. K. Sinclair and J. I. Skullerud, arXiv:1109.1475 [hep-ph].

- [44] W. E. Caswell, G. P. Lepage, Phys. Lett. **B167** (1986) 437.
- [45] G. P. Lepage *et al*, Phys. Rev. D **46** (1992) 4052 [arXiv:hep-lat/9205007].
- [46] G. T. Bodwin, E. Braaten and G. P. Lepage, Phys. Rev. D **51** (1995) 1125 [Erratum-ibid. D **55** (1997) 5853] [arXiv:hep-ph/9407339].
- [47] N. Brambilla, A. Pineda, J. Soto and A. Vairo, Rev. Mod. Phys. **77** (2005) 1423 [arXiv:hep-ph/0410047].
- [48] T. Umeda, Phys. Rev. D **75** (2007) 094502 [arXiv:hep-lat/0701005].
- [49] G. Aarts and J. M. Martínez Resco, JHEP **0204** (2002) 053 [arXiv:hep-ph/0203177].
- [50] P. Petreczky, Eur. Phys. J. C **62** (2009) 85 [arXiv:0810.0258 [hep-lat]].
- [51] G. Aarts, C. Allton, J. Foley, S. Hands and S. Kim, Phys. Rev. Lett. **99** (2007) 022002 [arXiv:hep-lat/0703008].
- [52] R.K. Bryan, Eur. Biophys. J. **18** (1990) 165.
- [53] S. Caron-Huot, M. Laine, G. D. Moore, JHEP **0904** (2009) 053 [arXiv:0901.1195 [hep-lat]].
- [54] H. B. Meyer, New J. Phys. **13** (2011) 035008 [arXiv:1012.0234 [hep-lat]].
- [55] R. Morrin, A. Ó Cais, M. Peardon, S. M. Ryan and J. I. Skullerud, Phys. Rev. D **74** (2006) 014505 [arXiv:hep-lat/0604021].
- [56] C. T. H. Davies *et al*, Phys. Rev. D **50** (1994) 6963 [arXiv:hep-lat/9406017].
- [57] C. T. H. Davies, K. Hornbostel, G. P. Lepage, A. J. Lidsey, J. Shigemitsu and J. H. Sloan, Phys. Rev. D **52** (1995) 6519 [arXiv:hep-lat/9506026].
- [58] C. T. H. Davies *et al* [UKQCD Collaboration], Phys. Rev. D **58** (1998) 054505 [arXiv:hep-lat/9802024].
- [59] G. P. Lepage and P. B. Mackenzie, Phys. Rev. D **48** (1993) 2250 [arXiv:hep-lat/9209022].
- [60] P. Petreczky, S. Datta, F. Karsch, I. Wetzorke, Nucl. Phys. Proc. Suppl. **129** (2004) 596-598. [hep-lat/0309012].
- [61] K. Nakamura [Particle Data Group], J. Phys. G **37** (2010) 075021.
- [62] I. Adachi et al [Belle Collaboration], arXiv.1103.3419.

- [63] F. Karsch, E. Laermann, P. Petreczky, S. Stickan, Phys. Rev. **D68** (2003) 014504 [hep-lat/0303017].
- [64] G. Aarts, J. M. Martínez Resco, Nucl. Phys. **B726** (2005) 93-108 [hep-lat/0507004].